Received May 2004
Revised July 2005
Accepted July 2005

An advanced impingement/film cooling scheme for gas turbines – numerical study

A. Immarigeon and I. Hassan
Department of Mechanical and Industrial Engineering, Concordia University, Montréal, Canada

Abstract

Purpose – The present study aims to conduct a numerical investigation of a novel film cooling scheme combining in-hole impingement cooling and flow turbulators with traditional downstream film cooling, and was originally proposed by Pratt & Whitney Canada for high temperature gas turbine applications.

Design/methodology/approach – Steady-state simulations were performed and the flow was considered incompressible and turbulent. The CFD package FLUENT 6.1 was used to solve the Navier-Stokes equations numerically, and the preprocessor, Gambit, was used to generate the required grid.

Findings – It was determined that the proposed scheme geometry can prevent coolant lift-off much better than standard round holes, since the cooling jet remains attached to the surface at much higher blowing rates, indicating a superior performance for the proposed scheme.

Research limitations/implications – The present study was concerned only with the downstream effectiveness aspect of performance. The performance related to the heat transfer coefficient is a prospective topic for future studies.

Practical implications – Advanced and innovative cooling techniques are essential in order to improve the efficiency and power output of gas turbines. This scheme combines in-hole impingement cooling and flow turbulators with traditional downstream film cooling for improved cooling capabilities.

Originality/value – This new advanced cooling scheme both combines the advantages of traditional film cooling with those of impingement cooling, and provides greater airfoil protection than traditional film cooling. This study is of value for those interested in gas turbine cooling.

Keywords Films (states of matter), Cooling, Gas flow, Flow measurement, Computational geometry

Paper type Research paper

Nomenclature

D_h = hydraulic diameter of cavity hole at exit plane (m)
k = turbulent kinetic energy (m^2/s^2)
L = length of injection impingement hole (m)
M = blowing ratio (or rate) ($M_i = \rho_{j_i} U_{j_i}/\rho_\infty U_\infty$, $M_e = \rho_{j_e} U_{j_e}/\rho_\infty U_\infty$)
T = temperature (K)
T_{aw} = adiabatic wall temperature (K)
$\overline{T}_{aw}$ = spanwise averaged adiabatic wall temperature (K)
Ti = turbulence intensity
U = velocity (m/s)
x = streamwise distance measured from center of cavity outlet (m)
y = vertical distance measured from the test surface (m)
y^+ = non-dimensional wall distance ($y^+ = \rho u_\tau y_p/\mu$)
z = vertical distance measured from the cavity outlet centerline plane (m)

International Journal of Numerical Methods for Heat & Fluid Flow
Vol. 16 No. 4, 2006
pp. 470-493

0961-5539
DOI 10.1108/09615530610653091

Greek symbols

α = injection (or inclination) angle for holes

β = orientation angle for holes

ε = dissipation rate of turbulent kinetic energy (m^2/s^3)

η = local adiabatic film cooling effectiveness, ($\eta = (T_{aw} - T_\infty)/(T_j - T_\infty)$)

$\overline{\eta}$ = spanwise averaged film cooling effectiveness, ($\overline{\eta} = (\overline{T}_{aw} - T_\infty)/(T_j - T_\infty)$)

ρ = density (kg/m^3)

Subscripts and superscripts

aw = adiabatic wall

e = exit conditions

i = inlet conditions

j = refers to the jet

w = wall conditions

∞ = mainstream conditions at inlet plane and in free stream

1. Introduction

Advanced and innovative cooling techniques are essential in order to improve the efficiency and power output of gas turbines. Turbine inlet temperatures of 1,600 K are typical for current gas turbines, and there is an interest in increasing the temperatures for the next generation of gas turbines. Over the past decades, significant effort has been devoted to developing effective cooling strategies to maintain the blade temperature below the melting point of alloys used to construct the airfoils. As a result, various cooling strategies have been developed such as film, impingement and multi-pass cooling.

Many experimental and computational studies have been conducted in order to study the cooling process of gas turbine blades, understand this complex flow and heat process, and devise the best possible cooling schemes. Methods that have been mainly investigated include film cooling (Hyams and Leylek, 2000; Cho *et al.*, 2001; Gartshore *et al.*, 2001; Goldstein and Jin, 2001; Cutbirth and Bogard, 2002), impingement cooling (Son *et al.*, 2001; Taslim *et al.*, 2001), and advanced internal or external cooling (Azad *et al.*, 2000; Taslim *et al.*, 2001). These methods are commonly studied with the following parameters: injection orientations (Brittingham and Leylek, 2000; Jung and Lee, 2000; Gritsch *et al.*, 2001; Dittmar *et al.*, 2003), hole length (Burd *et al.*, 1998; Harrington *et al.*, 2001), free stream turbulence (Ekkad *et al.*, 1998; Mayhew *et al.*, 2003; Saumweber *et al.*, 2003), hole entrance effects (Hale *et al.*, 2000; Wilfert and Wolff, 2000; Gritsch *et al.*, 2003), hole exit tapering (Kohli and Bogard, 1999; Sargison *et al.*, 2002), hole exit expanding (Gritsch *et al.*, 2003; York and Leylek, 2003; Kim and Kim, 2004) and density ratio effects (Ekkad *et al.*, 1998). Only recent references have been given here, and earlier reports may be traced through the reference lists of the papers cited. From these reports and their references, some broad generalizations can be made about the methods, geometries, and conditions most appropriate for internal or external cooling of gas turbine blades:

- Hole geometry is an important parameter for film cooling performance. Laterally-and-forward-expanded holes provide higher values of spanwise averaged effectiveness and lower values of spanwise averaged heat transfer coefficients than laterally-expanded holes. However, the former has a tendency to allow hot mainstream ingestion into the windward portion of the hole exit. Flared holes have the best overall performance, especially at high blowing rates, when compared to the standard circular film cooling hole. Their diffused exits reduce

the coolant momentum, allowing it to spread laterally, thus resulting in increased film protection.

- Compound angle injection, whether for shaped or circular holes, leads to an increase in spanwise averaged effectiveness compared to that obtained with standard circular holes. However, compound jets generally produce higher values of heat transfer coefficient on the surface than do simple injection jets, and this trend is amplified as the blowing rate rises.
- Hole spacing affects the ability of adjacent jets to coalesce. Small hole spacing results in better coverage of the wall, and thus higher effectiveness values than larger ones. A pitch-to-diameter ratio of three was commonly used in film cooling studies.
- For standard circular holes on a flat surface with low mainstream turbulence intensities, the downstream effectiveness is optimum for blowing ratios of approximately 0.5. For blowing rates above this value, the coolant jet undergoes lift-off. This allows the hot gases to come in contact with the surface, which causes the effectiveness to decrease.
- At small blowing rates, the length-to-diameter ratio L/D_h generally has no major effect on the spanwise averaged effectiveness obtained for standard circular holes in a flat plate. The only exception is in the near-hole region where short holes perform best. At high blowing rates, small L/D_h holes, where $x/D_h \leq 3$, perform better in terms of effectiveness in the near-hole region, however, large L/D_h holes are more efficient further downstream. The smaller the hole length-to-diameter (L/D_h) ratio, the larger the effective injection angle, indicating that the jet lifts off at a smaller value of blowing ratio when the L/D_h ratio is small.
- An increase in mainstream turbulence intensity, Ti, at low blowing rates decreases the spanwise averaged adiabatic film cooling effectiveness due to the enhanced mixing of the mainstream and coolant flow. There is a critical blowing ratio for which an increase in Ti causes an increase in spanwise averaged effectiveness. For these cases, the turbulence delays the jet lift-off by pushing the detached jet back to the surface, which enhances the film coverage. Furthermore, the effectiveness is not as dependent on Ti at high blowing rates as it is at low blowing rates.
- A decrease in density ratio causes an increase in the downstream heat transfer coefficient on the film cooled surface for the 35° inclined holes, however, no significant effect on heat transfer coefficient for 90° inclined holes (normal injection) was observed. Lowering the density ratio has the same effect as increasing the momentum flux ratio, such that it reduces the lateral spreading of the jet thus lowering the spanwise averaged adiabatic film cooling effectiveness.
- All plenums with flow direction were observed to yield superior effectiveness compared to that for the standard stagnant plenum. The plenum flow direction has an effect on cooling effectiveness only when the plenum height is less than 2D. Counter-flow plenums produce better centerline effectiveness in the near-hole region than that in co-flow plenums at low and high blowing rates. However, at

high blowing rates, the co-flow performs best in terms of spanwise averaged effectiveness for $x/D_h \geq 2$.

Few studies in the open literature have focused on novel cooling schemes for increased cooling performance. To date, most film cooling schemes aim to cool the turbine airfoil surface downstream of injection. With the conception of the proposed advanced cooling scheme, a greater portion of the airfoil is protected. This scheme combines both the advantages of traditional film cooling with those of impingement cooling, and was originally proposed by Pratt & Whitney Canada. The film hole that transports coolant fluid from the inside to the outside of the blade is designed in such a way that the coolant must go through a bend before exiting the blade, as shown in Figure 1, thus impinging on the blade material. Furthermore, flow turbulators or pin fins are located on the path of the coolant in the louver, so as to increase the heat transfer even further. Finally, the flow exits very close to the blade surface, minimizing aerodynamic losses. The present study will numerically investigate the effect of the blowing ratio, the film hole geometry (impingement jet inlet geometry and pedestal configuration), the mainstream turbulence intensity, and the turbulence model on the downstream adiabatic film cooling effectiveness for such a geometry. The velocity, temperature, and turbulent kinetic energy fields will also be analyzed and reported in order to explain the behavior of the flow. While the impingement jet inlet geometry is expected to mainly affect the heat transfer characteristics of the impinging jet, it is expected that this geometry will also influence the downstream effectiveness.

2. Mathematical modeling and boundary conditions

The computational domain and film cooling geometries are shown in Figure 2. The domain consists of repeating sets of the holes-and-cavity configuration, such that

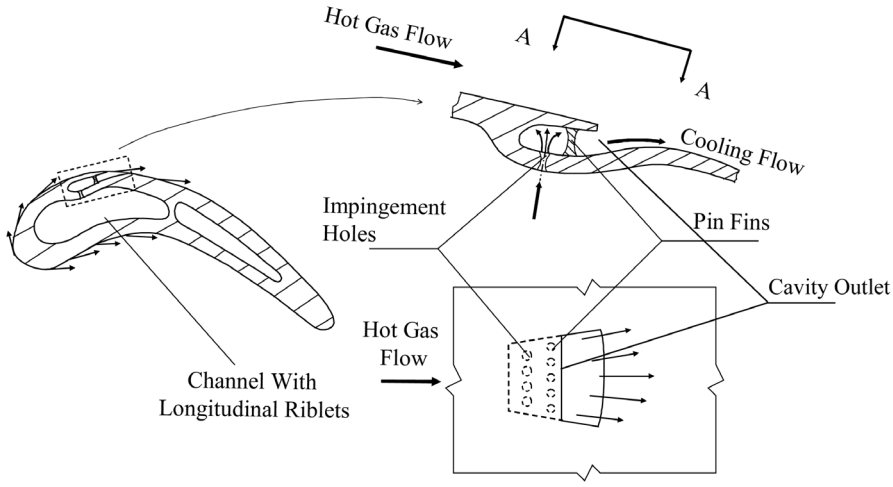

Figure 1.
Proposed cooling scheme

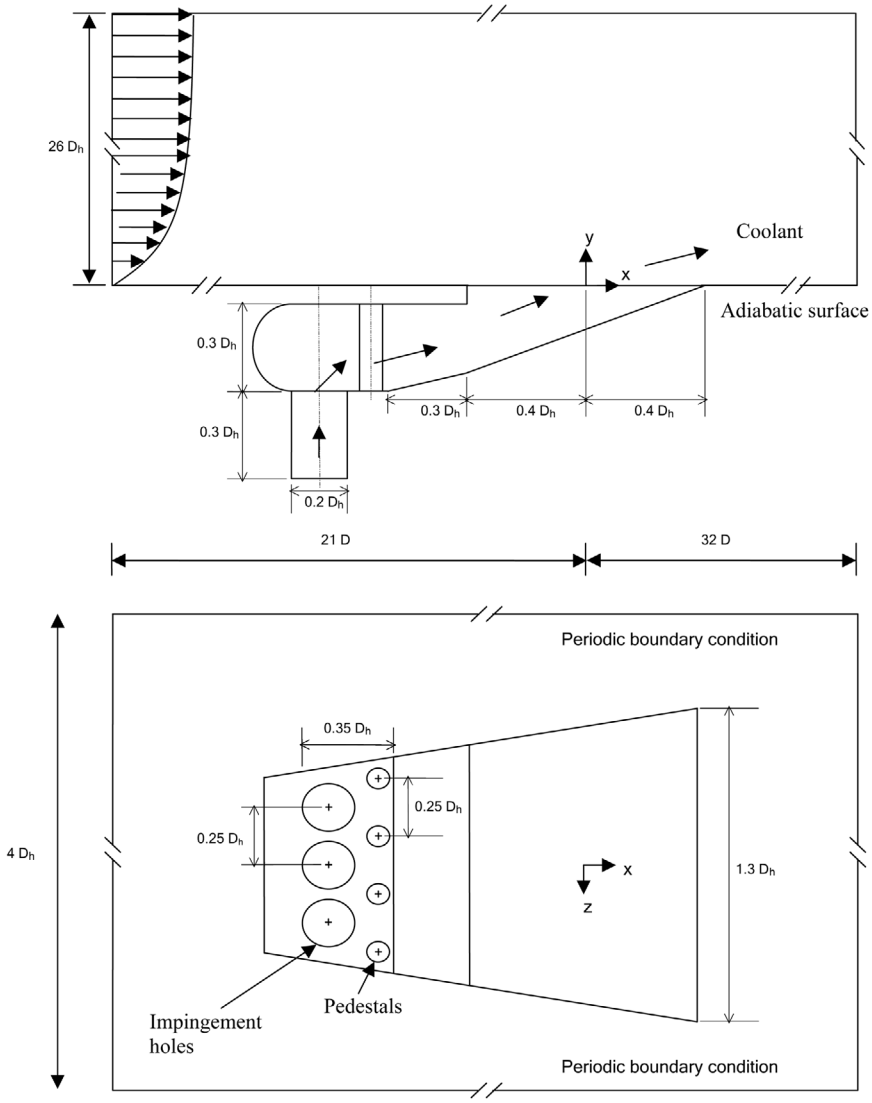

Figure 2.
Impingement-film-hole geometry (NOV1-4p configuration)

end-wall effects are neglected. The various hole configurations are summarized in Table I. Each case is designated by a two-part nomenclature. For example, NOV1-4p refers to the geometry possessing a three-impingement-hole inlet and four pedestals, as shown in Figure 2. The suffix refers to the pedestal configurations, with -4p, -2p and -0p corresponding to the four-pedestal, two-pedestal and no-pedestal arrangements, respectively. In the -2p configuration, the two outer pedestals have been removed. The computational domain extends $21D_h$ upstream, $32D_h$ downstream and $26D_h$ above the *locus* of injection, while the film hole pitch-to-diameter ratio is $4D_h$. Owing to the

periodic nature of the flow, the domain is centered about one film hole centerline and considered periodic about the planes $y/D_h = 2.0$ and $y/D_h = -2.0$. The film hole is oriented in the same direction as the mainstream flow.

Steady-state simulations were performed and the flow was considered incompressible and turbulent. For all cases studied, the mainstream and coolant inlet temperatures were set to 1,300 and 750 K, respectively. The coolant inlet velocity is maintained at 3 m/s, while the mainstream inlet velocity is varied between 1 and 6 m/s, corresponding to blowing rates M_i between 0.87 and 5.22, based on impingement hole inlet conditions. The zero-gradient condition was imposed for all dependent variables at the outlet boundary ($x/D_h = 32$) downstream from the jet center. The bottom wall and the injection duct walls were assumed to be adiabatic so zero heat flux was imposed. The top boundary was located at a distance $26D_h$ in the y-direction from the jet center, where an impermeable, free-slip condition was imposed.

The CFD package FLUENT 6.1 is used to solve the Navier-Stokes equations numerically. This CFD package uses the finite volume method and supports unstructured grids. It enables the use of different discretization schemes and solution algorithms, together with various types of boundary conditions. The pressure-implicit with splitting of operators algorithm was chosen as the pressure-velocity coupling method. This algorithm provides more efficient calculations than the SIMPLE and SIMPLEC algorithms, thus reducing the number of iterations required for convergence. The second-order upwind scheme was chosen in discretizing the equations. To ensure a good compromise between computing time using this discretization scheme and stability in the convergence process, under-relaxation factors between 0.3 and 0.7 were used. As part of the same CFD package, a preprocessor, Gambit, is used to generate the required grid for the solver. An unstructured grid of tetrahedral/wedge elements is used, with five layers of wedge-type mesh elements, placed adjacent to most wall surfaces to ensure a minimum of ten elements in the viscosity affected region. The wedge elements, unlike tetrahedral elements, have a fixed height on a given layer. This allows good control on element height to achieve a wall $y^+ \approx 1$, a condition related to the turbulence models used. The present grid arrangement (around 750,000 elements in the domain) was based on many preliminary grid dependence studies. A sample grid near the film hole region is shown in Figure 3. The criteria for convergence of the conservation equations were a reduction in the residuals by more than four orders of magnitude for each equation, and an imbalance in the mass flow rate at the film hole exit plane inferior to 10^{-5}.

Geometry	Description
NOV1-4p	Three inlet impingement holes Four pedestals
NOV1-2p	Three inlet impingement holes Two pedestals (the two outer pedestals are removed)
NOV1-0p	Three inlet impingement holes No pedestals
NOV2-4p	One inlet impingement slot Four pedestals

Table I.
Film cooling hole nomenclature

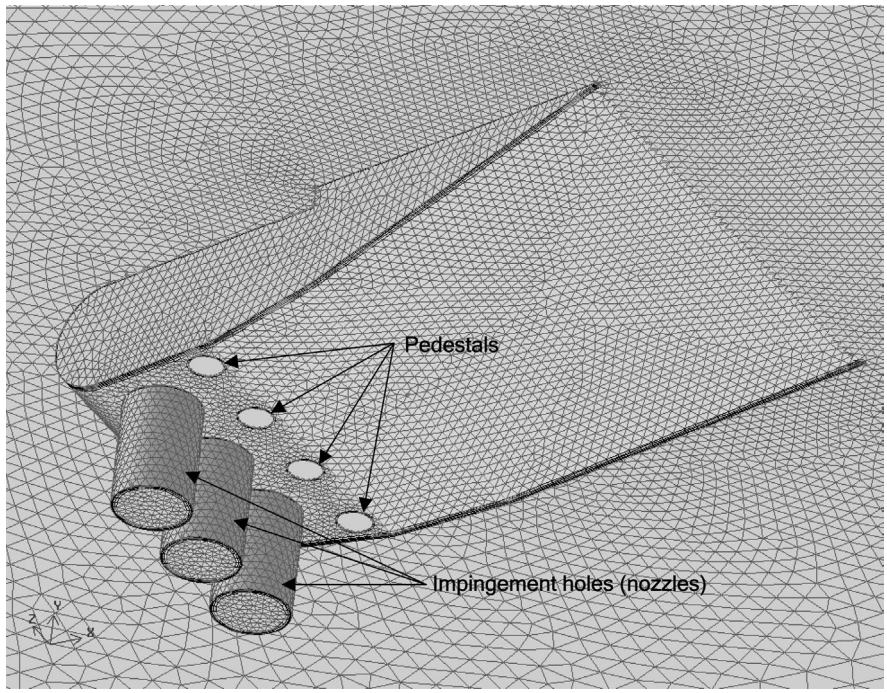

Figure 3.
Computational grid near-cavity hole region

Hale *et al.* (1999) evaluated several different turbulence models and wall function treatments available in the commercial CFD code FLUENT, assessing the ability of these combined models to predict the film cooling effectiveness for streamwise blowing from short injection holes (with $L/D_h = 2.91$, $\beta = 0°$ and $\alpha = 35°$ in the present notation) fed by a narrow plenum. The results of their study indicated that the use of usual wall functions to predict film cooling effectiveness in the near-hole region is problematic due to apparent boundary layer separation in that region. The use of two-layer zonal models improved the near-hole predictions considerably, and gave details of separation just downstream of the film holes which were not predicted by the usual engineering wall functions. However, no model of turbulence combined with any of the wall functions which they used was able to give adequate predictions over the entire region downstream of the film holes for their blowing ratios of 0.5 and 1.0. The failure of the usual turbulence models to predict measured values is likely to be due to the presence of gross unsteadiness in the flow fields, effects which are not modeled correctly by any two equation or higher order model. These models could still be used in exploring new designs or extending an existing knowledge.

In the present work, turbulence closure was achieved using three Reynolds-averaged Navier-Stokes turbulence models with enhanced wall treatment. These models, namely the standard k-ε model (Launder and Spalding, 1974), the renormalization group (RNG) k-ε model (Yakhot and Orszag, 1986) and the realizable k-ε model (Shih *et al.*, 1995), employ averaged governing equations to solve for the mean flow quantities. The predictions using these models were validated and

compared with the experimental data obtained by Sinha *et al.* (1991) in Figure 4. It was found that the realizable k-ε model provided the most appropriate prediction of centerline adiabatic film cooling effectiveness, followed closely by the RNG k-ε model. These two turbulence models were, therefore, used in most of the simulations in the present study.

3. Results and discussion

The spanwise-averaged adiabatic film cooling effectiveness downstream of injection, $\bar{\eta}$, represents the average adiabatic film cooling effectiveness in the z-direction measured at a given x/D_h. This parameter is found by determining the lateral (z-direction) distribution of temperature at the wall ($y/D_h = 0$) at a given x/D_h. The average temperature $\overline{T}_{aw}$ at this location is then substituted in the following equation to obtain $\bar{\eta}$:

$$\bar{\eta} = \frac{\overline{T}_{aw} - T_\infty}{T_j - T_\infty}$$

Temperature is sampled at typically 100 data points in the z-direction, and the average was computed using standard numerical integration schemes. The following sections present results obtained for two different impingement hole inlets, as well as three different pedestal arrangements, and were computed with three different turbulence models. The velocity field, turbulent kinetic energy field and temperature field at various locations in the domain are also presented in detail.

3.1 Effect of blowing ratio

In the present study, the blowing rate is calculated using conditions at the impingement hole inlet, since the complexity of the geometry renders the analytical

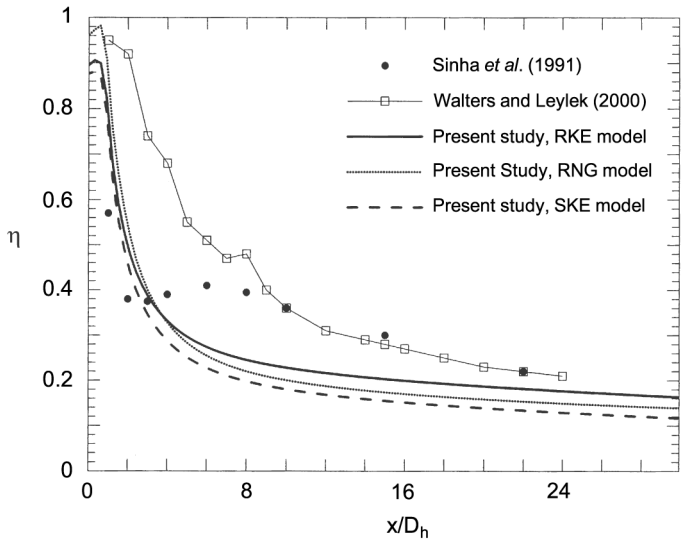

Figure 4.
Centerline adiabatic film cooling effectiveness for the simple injection circular hole, obtained with various turbulence models, at $M = 1.0$

calculation of jet exit conditions difficult. These conditions are different than those at the impingement hole inlet due to the changes in cross section of the hole. Based on impingement hole inlet conditions, the blowing ratio M_i varies between 0.87 and 5.22. More practically, this corresponds to a range of blowing rates M_e varying from 0.44 to 1.77, when the blowing rate is calculated based on film hole, or cavity outlet, exit conditions, i.e.

$$M_e = \frac{\rho_{j_e} U_{j_e}}{\rho_\infty U_\infty}$$

where ρ_{j_e} and U_{j_e} are the area-weighted average of density and velocity magnitude on the cavity outlet hole exit plane after computing the solution, respectively.

Figure 5 shows the downstream centerline adiabatic film cooling effectiveness obtained with the NOV1-4p geometry, at various blowing rates. All cases show a gradual decrease in effectiveness with increasing downstream position. As the blowing ratio M_i increases from 0.87 to 5.22 (equivalent to M_e increasing from 0.44 to 1.77), the centerline effectiveness increases or remains constant at all downstream positions. Many studies have shown that jet lift-off occurs for blowing rates of approximately 0.5 for cylindrical film cooling holes (Bergeles *et al.*, 1977). This is due to the fact that the hot mainstream gases are able to slip underneath the jet, thus reducing its cooling performance. In addition, the jet lift-off continues to intensify as the blowing rate increases beyond 0.5. With the present hole geometry, the coolant jet has not experienced any similar lift-off from the surface at any blowing rate studied, which would have otherwise caused a drop in centerline effectiveness in the near-hole region. The advantage of the forward expansion in the hole design is conveyed as an increased adherence of the film at high blowing rates. Owing to the flared cavity outlet, the coolant momentum is reduced, allowing it to spread laterally onto the surface, thus enhancing the cooling performance. The rate at which the centerline effectiveness decreases is reduced as the blowing ratio rises, according to Figure 5. As the coolant

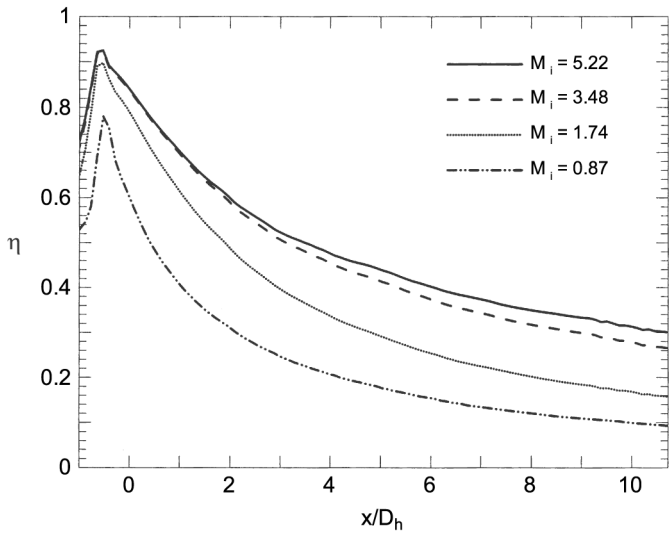

Figure 5.
Centerline adiabatic film cooling effectiveness for the NOV1-4p geometry at various M_i (Ti = 3 percent, realizable k-ε turbulence model)

gains momentum with respect to the mainstream, the jet dilution is delayed as more coolant is convected downstream. This provides an enhanced protection of the wall in the streamwise direction.

Figure 6 shows an overall outlook on the temperature field at various cross-stream planes downstream of injection at all blowing rates. The contours show the interaction of the coolant and mainstream flows, as well as the growing impact of the jet on the temperature field. The thermal dilution of the coolant resulting from the mixing between the coolant flow and the mainstream flow is visible at $x/D_h = 5$. The gradients of temperature at this location decrease and the film temperature is warmer than at injection, hence reducing the film effectiveness. The increase in lateral coolant coverage is most visible at $x/D_h = 3$ and $x/D_h = 5$. At $x/D_h = 1$, some lateral spreading is observed as the blowing rate increases from $M_i = 0.87$ to 3.48. When the blowing rate reaches 3.48, however, the lateral spreading levels out, while the jet continues to grow in the vertical direction. This contraction and rise of the jet, accompanied by a stall in the growth of centerline effectiveness as shown in Figure 5, denotes that jet lift-off is imminent at $x/D_h = 1$.

The lateral distribution of adiabatic film cooling effectiveness at various downstream positions is shown in Figure 7. For all blowing rates, the effectiveness increases at lateral positions while decreasing in the centerline as the distance increases from the injection *locus*. This jet spreading is due to a reduction in coolant momentum through dissipation losses, and induces a thinning of the jet in the centerline as the coolant travels to larger z/D_h values. Peaks of effectiveness, symmetrical about the centerline, are observed on the effectiveness distributions. These are most pronounced at $x/D_h = 1$, and move closer together as the blowing rate is increased. This is due to the jetting effect which prevents the coolant from spreading laterally. As M_i increases from 0.87 to 3.48, the reduction of the high effectiveness region between the peaks is offset by an overall rise in effectiveness values, so that the spanwise averaged effectiveness at $x/D_h = 1$ increases steadily. As M_i increases from 3.48 to 5.22, the peaks continue to move inwards, hence reducing the region of high effectiveness between them. However, the overall effectiveness does not increase enough to overcome this deficit, and this translates to a net decrease in spanwise averaged effectiveness at $x/D_h = 1$. The benefits of this high blowing ratio are observed far downstream of injection ($x/D_h = 10$), where the distribution of effectiveness is the highest over the widest span of all cases. Since, the jet core is larger, coolant dilution is hindered, and so the influence of the jet is felt at wider and longer distances downstream of injection. However, it also ensures less dilution of the jet, so that it is able to reach regions farther downstream of injection.

The peaks of effectiveness visible at the edges of the regions of high effectiveness, as shown in Figure 7, and are evidence that the flow does not exit the cavity outlet hole uniformly, especially at high blowing rates. This is confirmed when examining the contours of normalized velocity magnitude at the cavity outlet plane ($y/D_h = 0$) in Figure 8. The velocity magnitude is divided by the reference (main stream) velocity magnitude. The contours shown in this figure reveal that the jet exit velocity is relatively uniform at $M_i = 0.87$, but as the blowing rate increases, the coolant is redistributed and the jet exits mainly in the leeward and centerline portion of the film hole. At $M_i = 0.87$, the mainstream momentum is comparatively large with respect to that of the coolant. Crossflow blockage prevents the coolant from penetrating into the

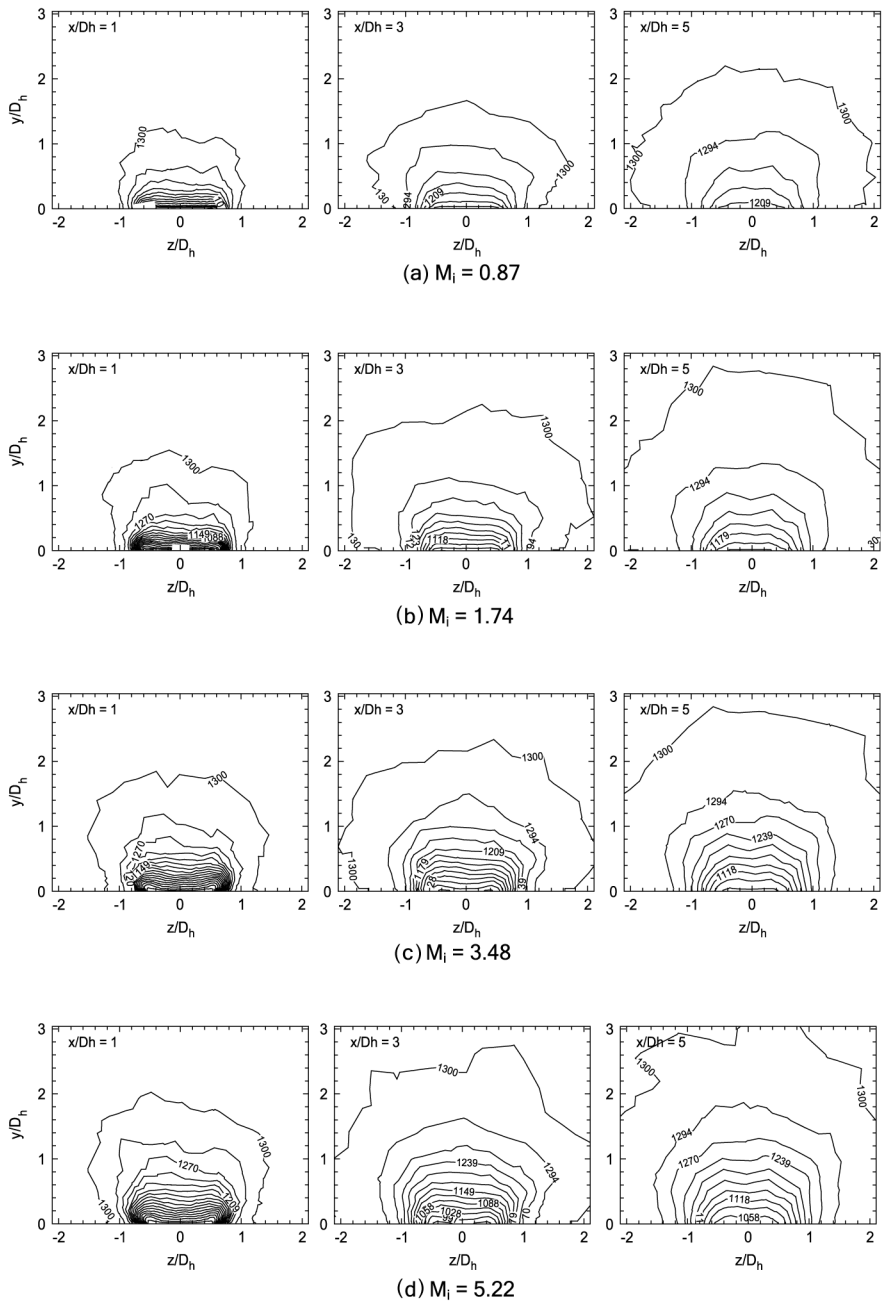

Figure 6.
Temperature contours on planes downstream of injection, at various blowing rates (NOV1-4p, Ti = 3 percent, realizable k-ε turbulence model)

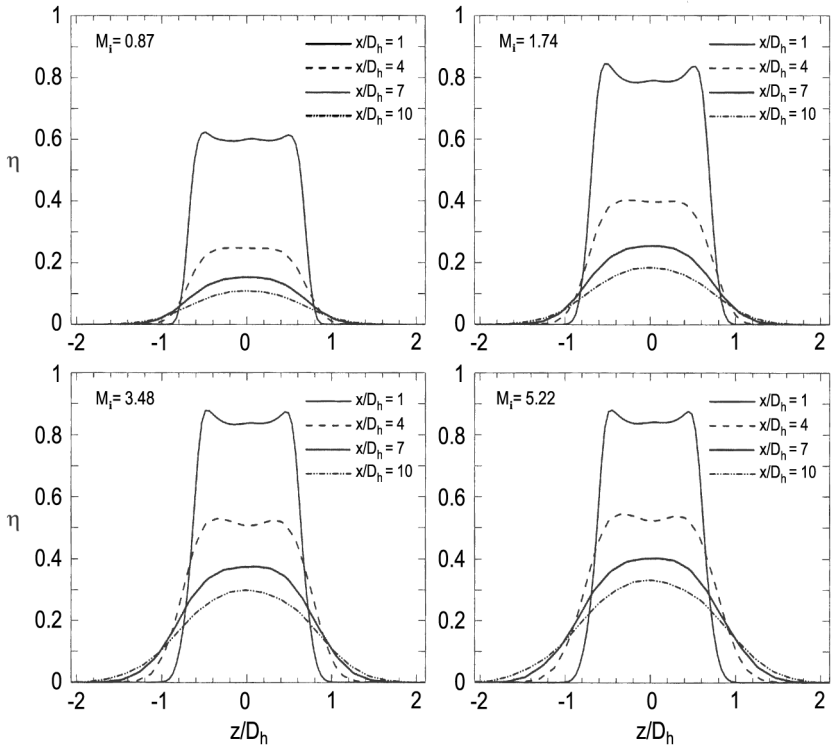

Figure 7.
Spanwise distribution of adiabatic film cooling effectiveness at various downstream positions and for all blowing rates (NOV1-4p, Ti = 3 percent, realizable k-ε turbulence model)

mainstream up to a certain degree. The mainstream/coolant interactions are minimum, and the coolant velocity assumes a relatively homogeneous distribution at the cavity outlet. As the jet momentum increases, the mainstream blockage becomes less significant. Owing to the reduced constraint, the coolant shoots out of the cavity outlet in the centerline with a rising trajectory instead of expanding along the sides of the outlet. Figure 8 also shows that the flow accelerates along the edges of the film hole, especially at high blowing ratio. This phenomenon is caused by the blockage brought on by the presence of the jet inside the mainstream. The coolant jet is a growing obstacle in the mainstream as the blowing rate increases, much like a cylinder in crossflow. As the jet becomes higher and stronger, it diverts the mainstream, which must accelerate around its edges in order to satisfy continuity. This phenomenon also generates secondary flow (vortices) in the wake region of the jet.

3.2 Effect of pedestals

It can be foreseen that the presence of pedestals will change the structure of the flow. This section will investigate the degree to which these flow turbulators alter the flow patterns. Figure 9 shows contours of normalized velocity magnitude on the cavity outlet plane at $M_i = 5.22$, for the NOV1-4p, NOV1-2p and NOV1-0p geometries. This figure confirms that the coolant flow is indeed disturbed by the presence of the

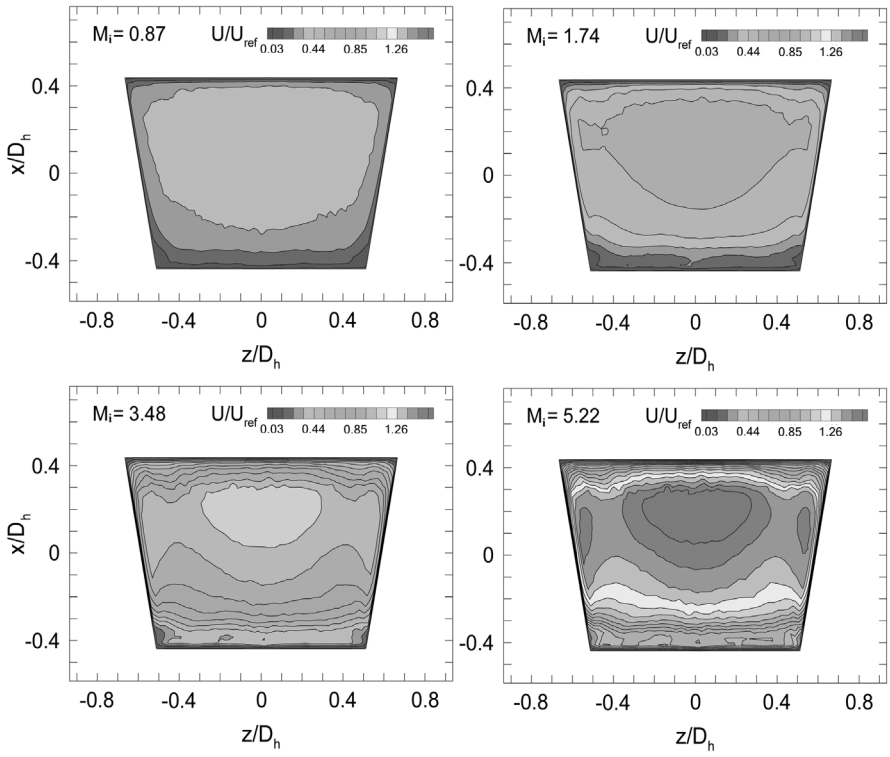

Figure 8.
Normalized velocity magnitude contours on the cavity outlet plane for all blowing rates (NOV1-4p, Ti = 3 percent, realizable k-ε turbulence model)

pedestals. As opposed to the NOV1-4p case, where the flow exits mainly in the leeward and centerline portion of the cavity, the flow is forced to accelerate along the sides of the cavity in the NOV1-2p case. Owing to the absence of side pedestals, the coolant tends to bypass the two center pedestals, thus deflecting towards the walls of the cavity, and therefore, slowing down due to the expansion of the cavity. In the NOV1-0p case, the velocity distribution at the cavity outlet is the most uniform of all three cases at this blowing rate. The three coolant jets originating from the impingement tubes coalesce to form two median streams and two outer streams. This is due to the increase in cross-sectional area inside the cavity. The flow of the coolant mostly follows the gradual expansion of the cavity. However, the jet originating from the middle impingement tube separates into two streams in an attempt to expand to the sidewall. These streams entrain the innermost part of the fluid from the other two jets, and exit around the midline of the cavity. In terms of centerline effectiveness, the NOV1-2p configuration is the most effective design, since lower centerline velocity promotes less mixing of the coolant and hence produces a more effective film protection.

Figure 10 shows the contours of normalized streamwise velocity in the centerline for the three pedestals configurations at $M_i = 5.22$. The contours show a substantial increase in streamwise velocity for the NOV1-4p case, as compared to the case where the cavity contains no pedestals. This is due to the bulk of the coolant exiting in the centerline in the NOV1-4p case. However, for the NOV1-2p case, the velocity contours

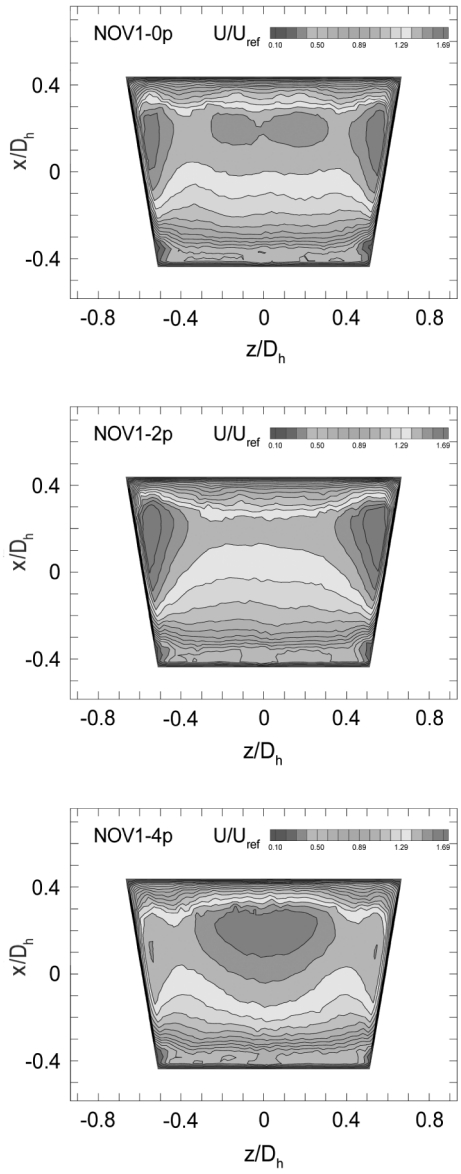

Figure 9.
Normalized velocity magnitude contours on the cavity outlet plane for three pedestal configurations ($M_i = 5.22$, Ti = 3 percent, realizable k-ε turbulence model)

show a slower centerline flow than for the NOV1-0p case, since the flow is deviated towards the edges of the cavity by the two center pedestals. Figure 11 shows contours of normalized vertical and lateral velocity at $x/D_h = 1$ for the three pedestal configuration. The coolant for the four-pedestal geometry tends to spread more laterally and remains closer to the surface than for the other cases. Even though the centerline velocity magnitude is highest for the NOV1-4p case, the penetration is lowest

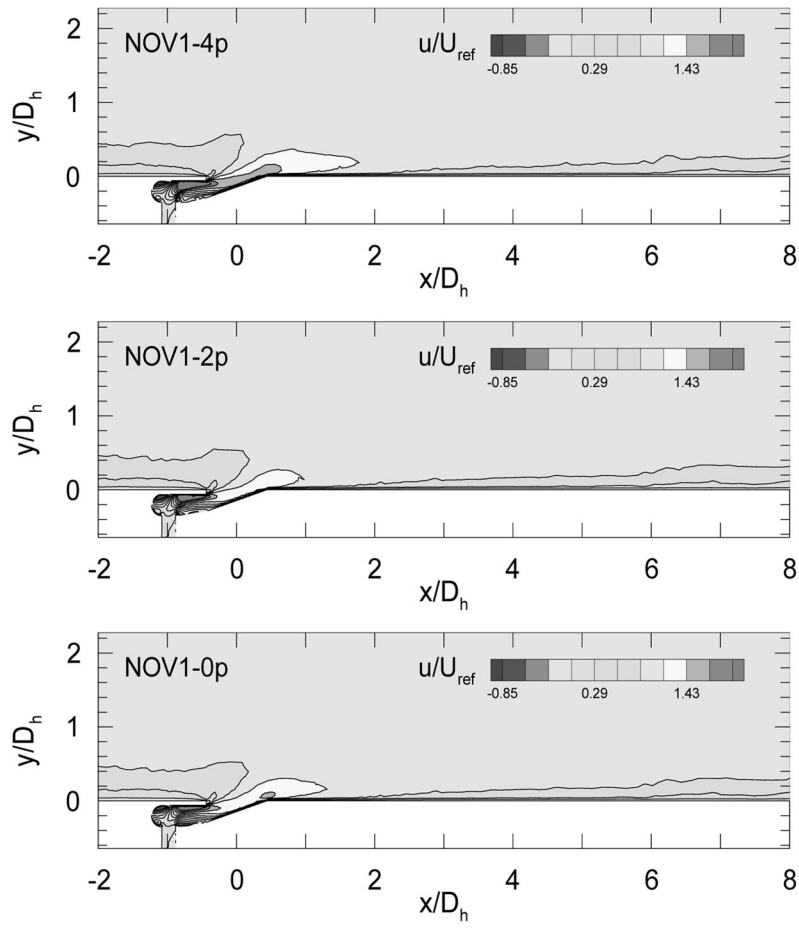

Figure 10.
Contours of the normalized streamwise velocity in the centerline plane for three pedestal configurations ($M_i = 5.22$, Ti = 3 percent, realizable k-ε model)

as the coolant changes direction quickly after being injected into the mainstream. Both the NOV1-2p and NOV1-0p configurations produce a coolant jet with a trajectory 20 percent higher than that for the NOV1-4p arrangement at $x/D_h = 1$ (Figure 11(a)). The contours on Figure 11(b) prove that the lateral velocity at $x/D_h = 1$ for the NOV1-4p case is overall the highest. This increased lateral momentum deprives the centerline of coolant, thus rendering the film thinner there, and resulting in lower centerline effectiveness. The coolant for the NOV1-2p case displays the least amount of spreading, from the low contours of lateral velocity as shown in Figure 11(b). Combined with a low centerline streamwise velocity, this indicates that the film protection at the centerline is superior to that for both the NOV1-0p and NOV1-4p cases.

The centerline adiabatic film cooling effectiveness obtained for schemes with four pedestals (NOV1-4p), two pedestals (NOV1-2p) and no pedestals (NOV1-0p), at high and low blowing rates, is shown in Figure 12. For $M_i = 0.87$, there is a very slight

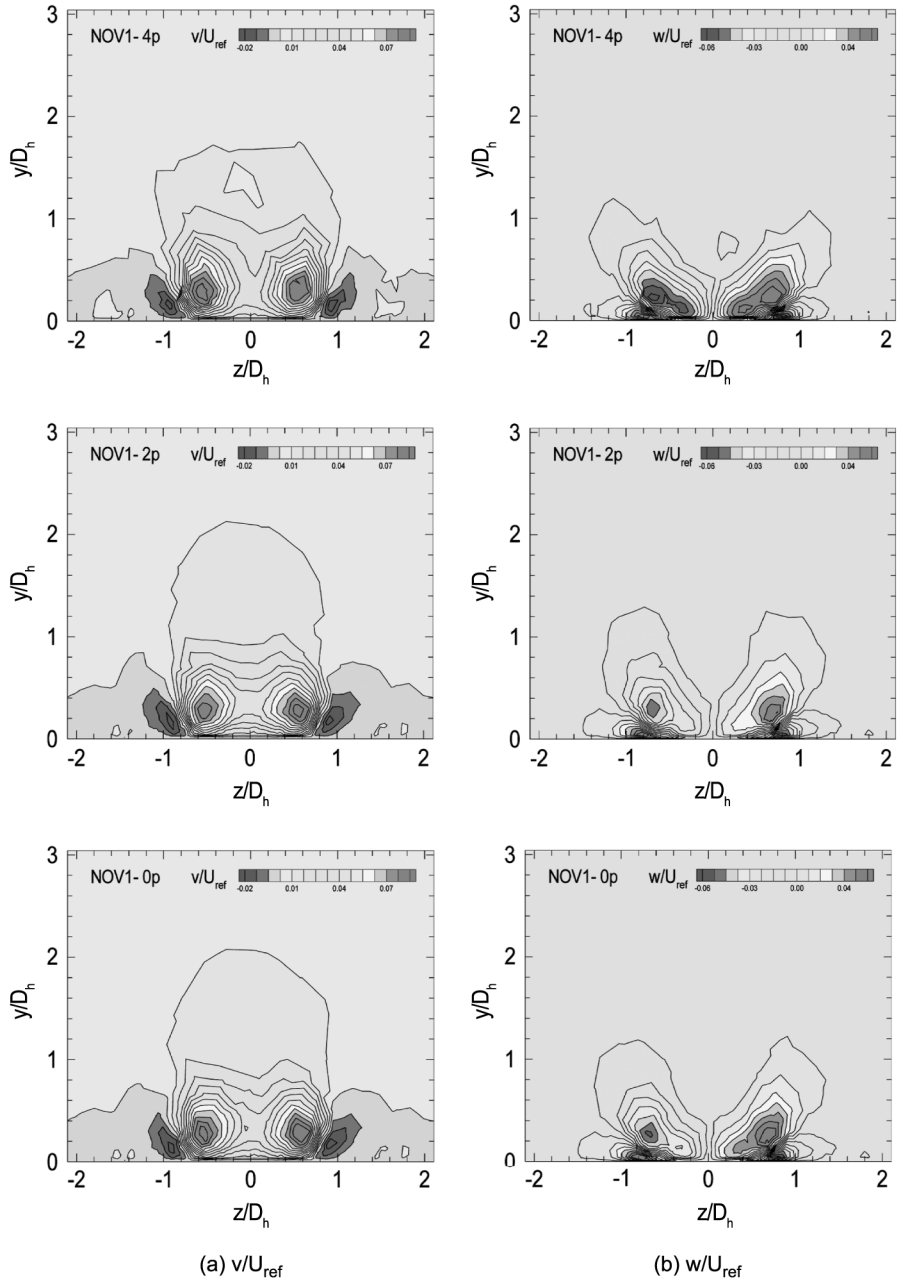

Figure 11.
Contours of velocity components at $x/D_h = 1$, for three pedestal configurations: (a) vertical normalized velocity; (b) lateral normalized velocity ($M_i = 5.22$, Ti = 3 percent, realizable k-ε turbulence model)

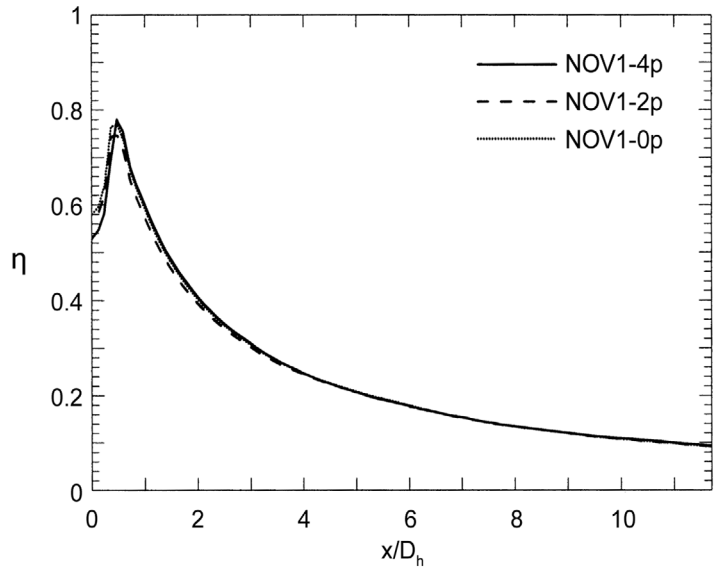

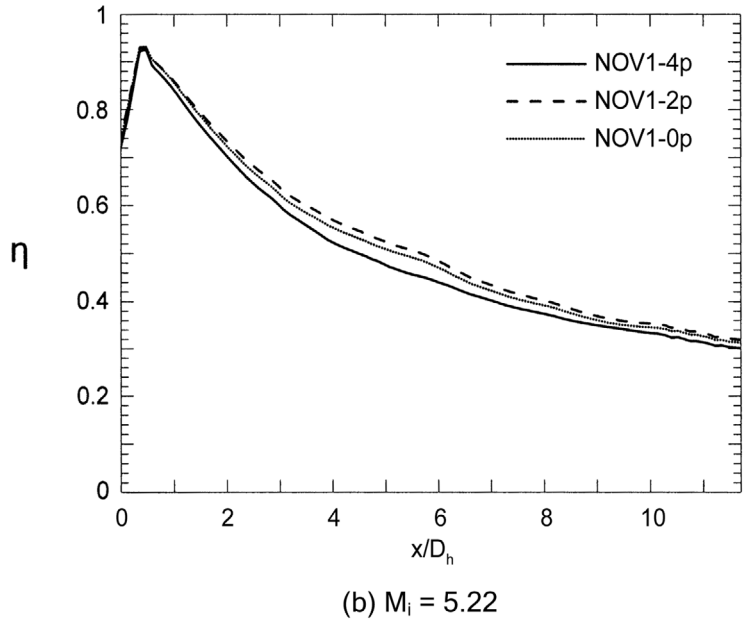

Figure 12.
Centerline adiabatic film cooling effectiveness for three pedestal configurations: (a) $M_i = 0.87$; (b) $M_i = 5.22$ (Ti = 3 percent, realizable k-ε turbulence model)

discrepancy in the centerline effectiveness for $x/D_h \leq 4$ obtained with the three geometries. Further downstream, the difference in results is considered to be negligible. At $M_i = 5.22$, the highest centerline adiabatic film cooling effectiveness is attributed the NOV1-2p scheme configuration. Figure 13 shows the lateral distribution of effectiveness at various downstream positions obtained at $M_i = 5.22$, for the three pedestal configurations. According to these plots, the effectiveness in the centerline is systematically lowest for the NOV1-4p geometry. It was noticed that the four pedestals enhance the lateral spreading of the coolant at $x/D_h = 1$, thus increasing interaction between the mainstream and coolant and degrading the performance of the film at this location. The drawback of this mixing is offset by the ability of the jet to cover a wider surface as it moves further downstream. This translates into higher values of effectiveness at lateral positions for the NOV1-4p geometry, visible at $x/D_h = 4$, 7, and 10. The three configurations result in similar spanwise averaged effectiveness at low blowing rate. For $M_i = 5.22$, the difference in spanwise averaged effectiveness is insignificant except for $x/D_h \leq 2$. In the near-cavity hole region, the NOV1-2p configuration performs best because it promotes less mixing of the coolant with the mainstream. Farther downstream, the benefits and detriments for each case cancel each other out such that the film performance is essentially equivalent for all three configurations.

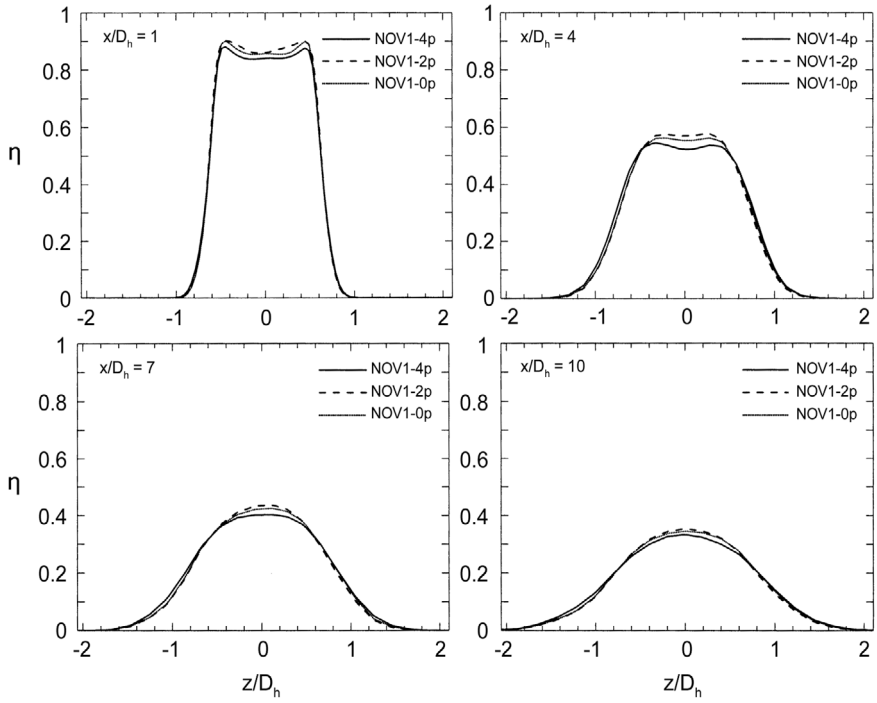

Figure 13.
Spanwise distribution of adiabatic film cooling effectiveness at various downstream positions for three pedestal configurations ($M_i = 5.22$, Ti = 3 percent, realizable k-ε model)

3.3 Effect of impingement hole inlet and turbulence models

The geometry of the inlet passage of the impingement hole is expected to influence the cooling performance of the flow. Obot *et al.* (1979) showed that the nozzle geometry has an effect on the heat transfer coefficient on an impingement plate in a simple impinging jet problem. The present study will only investigate the effect of the nozzle (or impingement hole inlet passage) geometry on the coolant downstream of injection in terms of adiabatic film cooling effectiveness. The cooling potential of the impingement jet for the inner blade material has not been investigated. The slot inlet geometry was tested at all blowing rates, namely, 0.87, 1.74, 3.48, and 5.22. The centerline adiabatic film cooling effectiveness obtained for each blowing rate is similar to those observed for the NOV1-4p geometry.

Figure 14 shows the normalized streamwise and vertical velocity contours at $x/D_h = 1$ for the NOV1-4p and NOV2-4p geometries. These contours show higher streamwise velocity concentrated in a smaller area for the NOV1-4p geometry. This denotes an overall narrower and faster jet core for this geometry than that for the NOV2-4p geometry. The vertical velocity contours in Figure 14(b) extend approximately 13 percent higher for the NOV2-4p than those for the NOV1-4p geometry, indicating that the jet height remains closer to the surface for the latter case. This suggests that the three discrete impingement nozzles act like flow separators which "pre-spread" the coolant laterally inside the cavity without losing momentum, so that it tends to remain closer to the wall and is faster once it exits into the mainstream. With a slot nozzle, the coolant exits though only one opening and loses momentum as it tries to fill the cavity. As the flow further expands laterally towards the sides of the cavity, the jet is depleted in the centerline, thus explaining the slower and larger jet just downstream of injection.

Figure 15 shows the downstream centerline effectiveness for the NOV1-4p geometry at $M_i = 0.87$ and 5.22, obtained using the three turbulence models mentioned above. For either blowing rate, the difference in centerline effectiveness was found to be lower than approximately 9 percent. In general, the RNG k-ε turbulence model yields the lowest prediction of centerline effectiveness of all three models for both blowing rates. The results obtained with the realizable and standard k-ε turbulence models are essentially the same at $M_i = 5.22$. However, at low blowing ratio, the realizable k-ε turbulence model gives a slightly higher prediction than the standard one for $x/D_h \leq 4$. Figure 16 shows contours of turbulent kinetic energy in the centerline plane obtained for the NOV1-4p geometry, with the three turbulence models. The contour plots show the high turbulent kinetic energy levels generated inside the cavity from the impingement process. Turbulent kinetic energy levels are also high near the injection *locus*, and are generated by a shearing process between the mainstream and the coolant. The turbulent kinetic energy is transported with the coolant as it is convected downstream, and dissipates through frictional losses incurred by the mainstream/coolant interactions. The contours of turbulent kinetic energy for the RNG case extend farther above the surface than for the other cases. This denotes that the RNG model overpredicts the turbulence levels in the coolant compared to the other models. This turbulence contributes to enhance the degree of mixing between the mainstream and the coolant, and also accelerates the dissipation of energy within the flow. This explains why the centerline effectiveness is almost always lower when using the RNG model than with the other models.

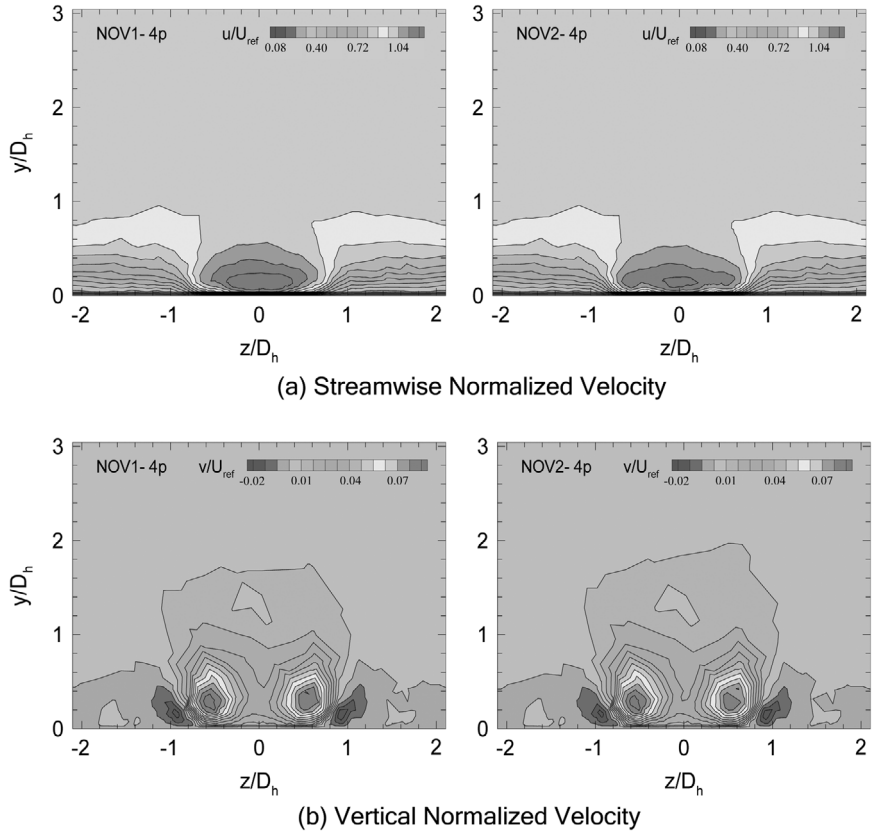

Figure 14.
Contours of velocity components at $x/D_h = 1$, for two impingement hole inlet geometries: (a) streamwise normalized velocity; (b) vertical normalized velocity ($M_i = 5.22$, Ti = 3 percent, realizable k-ε turbulence model)

4. Conclusions

A new film cooling scheme, originally proposed by Pratt & Whitney Canada, was tested at various flow conditions by means of computational simulations. This scheme combines in-hole impingement cooling and flow turbulators with traditional downstream film cooling for improved cooling capabilities. This study focused solely on the downstream cooling effectiveness aspect of performance with no investigation of heat transfer characteristics of the flow. The temperature, turbulence kinetic energy and flow fields were analyzed in centerline and spanwise planes in order to get a fundamental understanding of the cooling mechanisms. This is the first study in the open literature to investigate such a cooling scheme, and therefore, no experimental data were available for comparison purposes.

It was determined that the proposed scheme geometry can prevent coolant lift-off much better than standard round holes. While the cavity was tested for a large range of blowing rates, the centerline effectiveness obtained for each case, presented as a function of downstream position, increased or remained constant with increasing M_i. Results show that pedestals have a small effect on the spanwise averaged film cooling effectiveness at high blowing rate ($M_i = 5.22$) near the *locus* of injection ($x/D_h \leq 2$).

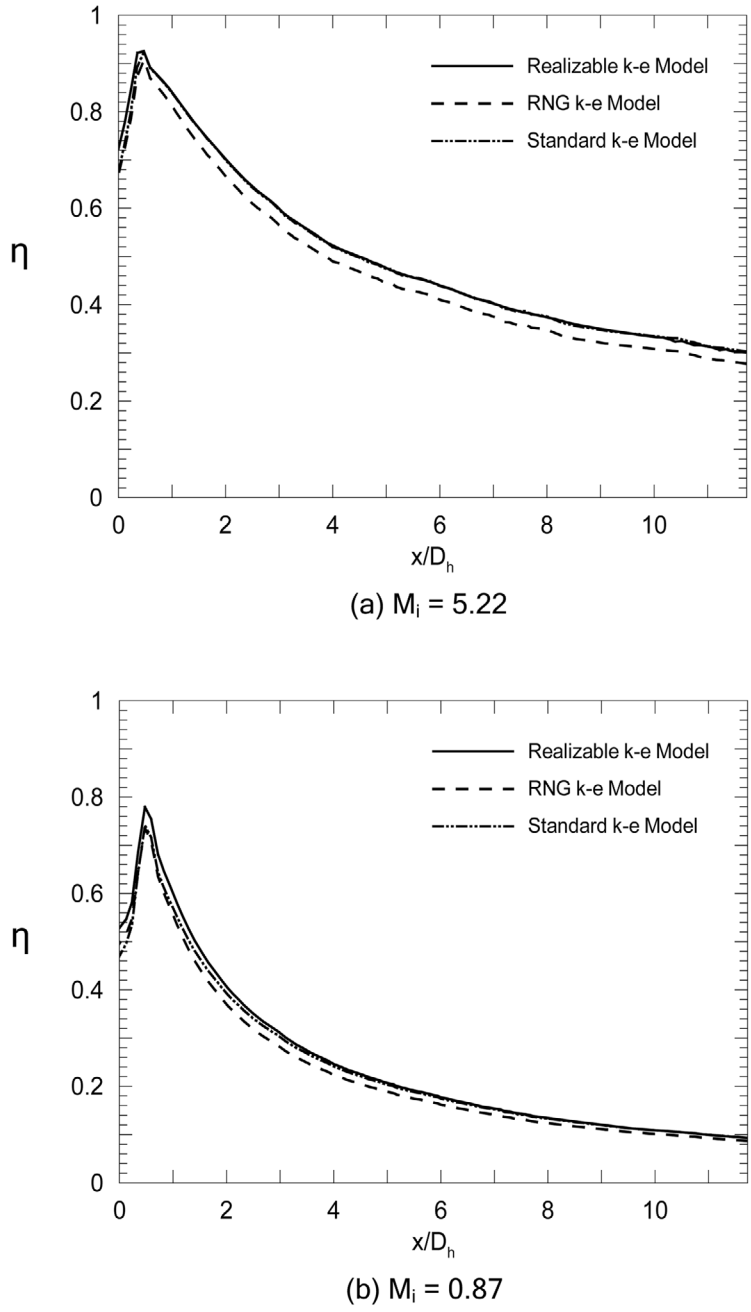

Figure 15.
Centerline adiabatic film cooling effectiveness for the NOV1-4p geometry, computed with various turbulence models for a mainstream turbulence intensity of 3 percent: (a) $M_i = 5.22$; (b) $M_i = 0.87$

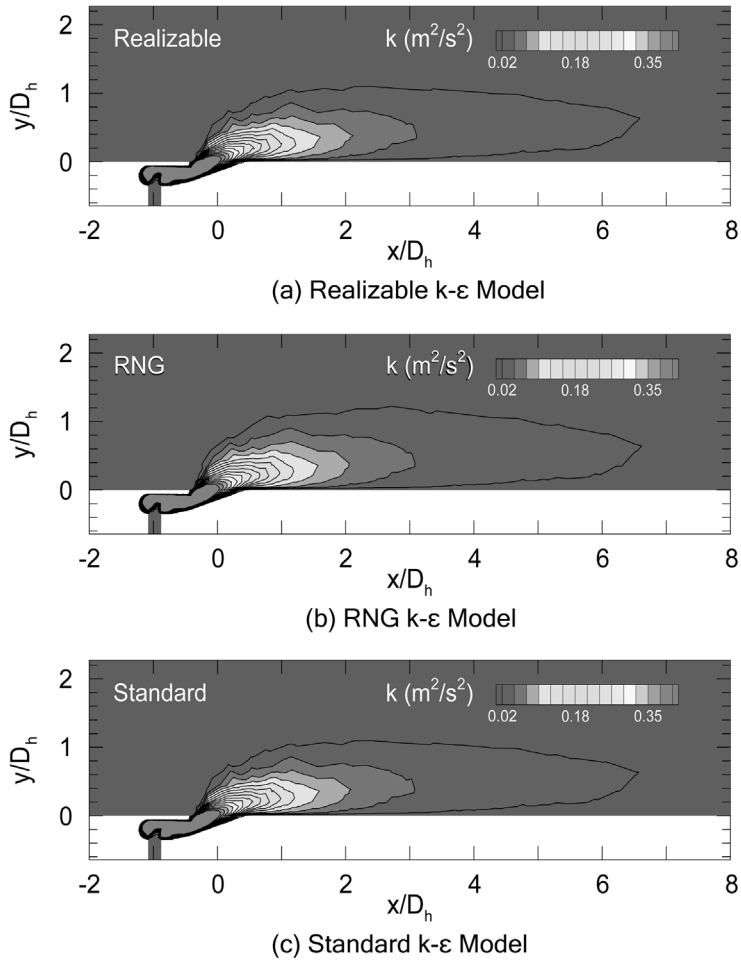

Figure 16.
Contours of the turbulent kinetic energy in the centerline plane computed with three turbulence models with enhanced wall treatment: (a) RKE Model; (b) RNG Model; (c) SKE Model (NOV1-4p, $M_i = 5.22$, Ti = 3 percent)

Depending on their arrangement, the pedestals act as a comb inside the cavity, thus altering the coolant distribution. The pedestals were found to help spread the coolant downstream of injection. While the four-pedestal configuration ensures a lower jet with more outwards momentum than for the other configurations, the two-pedestal configurations gives the best performance in terms of downstream effectiveness distributions, due to the lower levels of mixing it promotes within the mainstream.

The results presented in this work provide important insights for future studies of this scheme. The present study was only concerned with the downstream effectiveness aspect of performance. The performance related to the heat transfer coefficient is a prospective topic for future studies. In particular, the heat transfer characteristics of the impingement jet inside the cavity have an effect on the temperature of the target wall, thus influencing the performance of this cooling scheme overall. Future studies need to investigate how

these heat transfer characteristics are influenced by such parameters as the geometry of the nozzle. These findings will complement the results found in the present study and give a better overall understanding of the cooling performance using this scheme.

References

Azad, G.S., Han, J.C., Teng, S. and Boyle, R. (2000), "Heat transfer and pressure distributions on a gas turbine blade tip", *Journal of Turbomachinery*, Vol. 122, pp. 717-24.

Bergeles, G., Gosman, A.D. and Launder, B.E. (1977), "Near-field character of a jet discharged through a wall at 30 degrees to a mainstream", *AIAA Journal*, Vol. 15 No. 4, pp. 499-504.

Brittingham, R.A. and Leylek, J.H. (2000), "A detailed analysis of film cooling physics: Part IV – Compound-angle injection with shaped holes", *Journal of Turbomachinery*, Vol. 122, pp. 133-45.

Burd, S.W., Kaszeta, R.W. and Simon, T.W. (1998), "Measurements in film cooling flows: hole L/D and turbulence intensity", *Journal of Turbomachinery*, Vol. 120, pp. 791-8.

Cho, H.H., Rhee, D.H. and Kim, B.G. (2001), "Enhancement of film cooling performance using a shaped film cooling hole with compound angle injection", *JSME International Journal, Series B*, Vol. 44 No. 1, pp. 99-110.

Cutbirth, J.M. and Bogard, D.G. (2002), "Thermal field and flow visualization within the stagnation region of a film-cooled turbine vane", *Journal of Turbomachinery*, Vol. 124, pp. 200-6.

Dittmar, J., Schulz, A. and Wittig, S. (2003), "Assessment of various film-cooling configurations including shaped and compound angle holes based on large-scale experiments", *Journal of Turbomachinery*, Vol. 125, pp. 57-64.

Ekkad, S.V., Han, J.C. and Du, H. (1998), "Detailed film cooling measurements on a cylindrical leading edge model: effect of free-stream turbulence and coolant density", *Journal of Turbomachinery*, Vol. 120, pp. 799-807.

Gartshore, I., Salcudean, M. and Hassan, I. (2001), "Film cooling injection hole geometry: hole shape comparison for compound cooling orientation", *AIAA Journal*, Vol. 39 No. 8, pp. 1493-9.

Goldstein, R.J. and Jin, P. (2001), "Film cooling downstream of a row of discrete holes with compound angle", *Journal of Turbomachinery*, Vol. 123, pp. 222-30.

Gritsch, M., Schulz, A. and Wittig, S. (2001), "Effect of crossflows on the discharge coefficient of film cooling holes with varying angles of inclination and orientation", *Journal of Turbomachinery*, Vol. 123, pp. 781-7.

Gritsch, M., Schulz, A. and Wittig, S. (2003), "Effect of internal coolant crossflow on the effectiveness of shape film-cooling holes", *Journal of Turbomachinery*, Vol. 125, pp. 547-54.

Hale, C.A., Plesniak, M.W. and Ramadhyani, S. (2000), "Film cooling effectiveness for short film cooling holes fed by a narrow plenum", *Journal of Turbomachinery*, Vol. 122, pp. 553-7.

Hale, C.A., Ramadhyani, S. and Plesniak, M.W. (1999), "Film cooling effectiveness predictions for short holes fed by a narrow plenum", ASME Paper No. 99-GT-162.

Harrington, M.K., McWaters, M.A., Bogard, D.G., Lemmon, C.A. and Thole, K.A. (2001), "Full-coverage film cooling with short normal injection holes", *Journal of Turbomachinery*, Vol. 123, pp. 798-805.

Hyams, D.G. and Leylek, J.H. (2000), "A detailed analysis of film cooling physics: Part III Streamwise injection with shaped holes", *Journal of Turbomachinery*, Vol. 122, pp. 122-32.

Jung, I.S. and Lee, J.S. (2000), "Effects of orientation angles on film cooling over a flat plate: boundary layer temperature distributions and adiabatic film cooling effectiveness", *Journal of Turbomachinery*, Vol. 122, pp. 153-60.

Kim, Y.J. and Kim, S.M. (2004), "Influence of shaped injection holes on turbine blade leading edge film cooling", *International Journal of Heat and Mass Transfer*, Vol. 47, pp. 245-56.

Kohli, A. and Bogard, D.G. (1999), "Effects of hole shape on film cooling with large angle injection", ASME Paper 99-GT-165.

Launder, B.E. and Spalding, D.B. (1974), "The numerical computation of turbulent flows", *Computer Methods in Applied Mechanics and Engineering*, Vol. 3, pp. 269-89.

Mayhew, J.E., Baughn, J.W. and Byerley, A.R. (2003), "The effects of free-stream turbulence on film cooling adiabtaic effectiveness", *International Journal of Heat and Fluid Flow*, Vol. 24, pp. 669-79.

Obot, N.T., Majumdar, A.S. and Douglas, W.J.M. (1979), "The effect of nozzle geometry on impingement heat transfer under a round turbulent jet", ASME Paper 79-WA/HT-53.

Sargison, J.E., Guo, S.M., Oldfield, M.L.G., Lock, G.D. and Rawlinson, A.J. (2002), "A converging slot-hole film-cooling geometry – Part I Low-speed flat-plate heat transfer and loss", *Journal of Turbomachinery*, Vol. 124, pp. 453-60.

Saumweber, C., Schulz, A. and Wittig, S. (2003), "Free-stream turbulence effects on film cooling with shaped holes", *Journal of Turbomachinery*, Vol. 125, pp. 65-72.

Shih, T-H., Liou, W.W., Shabbir, A., Yang, Z. and Zhu, J. (1995), "A new k-ε eddy viscosity model for high Reynolds number turbulent flows", *Computers Fluids*, Vol. 24 No. 3, pp. 227-38.

Sinha, A.K., Bogard, D.G. and Crawford, M.E. (1991), "Film-cooling effectiveness downstream of a single row of holes with variable density ratio", *Journal of Turbomachinery*, Vol. 113, pp. 442-9.

Son, C., Gillespie, D., Ireland, P. and Dailey, G. (2001), "Heat transfer and flow characteristics of an engine representative impingement cooling system", *Journal of Turbomachinery*, Vol. 123, pp. 154-60.

Taslim, M.E., Setayeshgar, L. and Spring, S.D. (2001), "An experimental evaluation of advanced leading edge impingement cooling concepts", *Journal of Turbomachinery*, Vol. 123, pp. 147-53.

Wilfert, G. and Wolff, S. (2000), "Influence of internal flow on film cooling effectiveness", *Journal of Turbomachinery*, Vol. 122, pp. 327-33.

Yakhot, V. and Orszag, S.A. (1986), "Renormalization group analysis of turbulence. I. Basic theory", *Journal of Scientific Computing*, Vol. 1 No. 1, pp. 3-51.

York, W.D. and Leylek, J.H. (2003), "Leading-edge film-cooling physics Part III Diffused hole effectiveness", *Journal of Turbomachinery*, Vol. 125, pp. 252-9.

Corresponding author
I. Hassan can be contacted at: hassan@me.concordia.ca